Gas-phase CO2 toward massive protostars

Boonman, A.M.S.; Dishoeck, E.F. van; Lahuis, F.; Doty, S.D.

A&A 399, 1063–1072 (2003)
DOI: 10.1051/0004-6361:20021868

Astronomy & Astrophysics

Gas-phase CO_2 toward massive protostars⋆

A. M. S. Boonman[1], E. F. van Dishoeck[1], F. Lahuis[1,2], and S. D. Doty[3]

[1] Sterrewacht Leiden, PO Box 9513, 2300 RA Leiden, The Netherlands
[2] SRON National Institute for Space Research, PO Box 800, 9700 AV Groningen, The Netherlands
[3] Department of Physics and Astronomy, Denison University, Granville, Ohio 43023, USA

Received 4 November 2002 / Accepted 16 December 2002

Abstract. We present infrared spectra of gas-phase CO_2 around 15 μm toward 14 deeply embedded massive protostars obtained with the Short Wavelength Spectrometer on board the Infrared Space Observatory. Gas-phase CO_2 has been detected toward 8 of the sources. The excitation temperature and the gas/solid ratio increase with the temperature of the warm gas. Detailed radiative transfer models show that a jump in the abundance of two orders of magnitude is present in the envelope of AFGL 2591 at $T > 300$ K. No such jump is seen toward the colder source NGC 7538 IRS9. Together, these data indicate that gas-phase CO_2 shows the same evolutionary trends as CO_2 ice and other species, such as HCN, C_2H_2, H_2O, and CH_3OH. The gas-phase CO_2 abundance toward cold sources can be explained by gas-phase chemistry and possible freeze-out in the outer envelope. Different chemical scenarios are proposed to explain the gas-phase CO_2 abundance of 1–2 $\times 10^{-6}$ for $T > 300$ K and of $\sim 10^{-8}$ for $T < 300$ K toward AFGL 2591. The best explanation for the low abundance in the warm exterior is provided by destruction of CO_2 caused by the passage of a shock in the past, combined with freeze-out in the coldest part at $T < 100$ K. The high abundance in the interior at temperatures where all oxygen should be driven into H_2O is unexpected, but may be explained either by production of OH through X-ray ionization leading to the formation of abundant gas-phase CO_2, or by incomplete destruction of evaporated CO_2 for $T > 300$ K.

Key words. stars: formation – ISM: abundances – ISM: molecules – infrared: ISM – ISM: lines and bands – molecular processes

1. Introduction

Carbondioxide is predicted to be among the more abundant carbon- and oxygen-bearing gas-phase species in massive star-forming regions (e.g. Charnley 1997). However, the lack of a permanent dipole moment restricts observations of this molecule to infrared wavelengths. Due to its ubiquitous presence in the Earth's atmosphere, it was not until the launch of the Infrared Space Observatory (ISO) that a systematic search for CO_2 toward star-forming regions could be performed. Van Dishoeck et al. (1996) made the first search for gas-phase CO_2 in absorption toward a few deeply embedded massive protostars. Since then, ISO has detected gas-phase CO_2 toward many astronomical objects, including other massive protostars (Dartois et al. 1998; van Dishoeck 1998), planetary atmospheres, and Asymptotic Giant Branch stars (e.g. Lellouch et al. 2002; Justtanont et al. 1998; Cami et al. 2000).

Van Dishoeck et al. (1996) derive tentative gas-phase CO_2 abundances of $\sim 10^{-7}$ averaged over the line of sight. Somewhat higher abundances of a few times 10^{-7} are found in the direction of Orion-IRc2/BN, whereas more than an order of magnitude lower abundances are found toward the shocked regions Peak 1 and 2 (Boonman et al. 2003). Envelope models by Doty et al. (2002) predict abundances of a few times 10^{-8} for temperatures $\lesssim$100 K and a few times 10^{-7}–10^{-6} for $T \sim$ 100–300 K. Hot core models by Charnley (1997) also predict abundances of $\sim 10^{-7}$–10^{-6} for $T \sim$ 200–300 K. On the other hand, Charnley & Kaufman (2000) show that shocks containing a high H/H_2 ratio can destroy CO_2, giving a possible explanation for the lower abundances found for the Orion shocked regions. Similarly, low gas-phase CO_2 abundances of $\sim 10^{-8}$ are predicted by gas-grain chemistry in the post-shock gas for dark-cloud type environments (Charnley et al. 2001).

In addition to gas-phase CO_2, abundant CO_2 ice has been seen toward intermediate- to high-mass star-forming regions (de Graauw et al. 1996; D'Hendecourt et al. 1996; Gerakines et al. 1999; Nummelin et al. 2001). Abundances up to $\sim 10^{-5}$ have been found, much higher than the gas-phase CO_2 abundances. The ice abundances are highest for the coldest sources, implying that grain-mantle evaporation is important for the

Send offprint requests to: A. M. S. Boonman,
e-mail: boonman@strw.leidenuniv.nl

⋆ Based on observations with ISO, an ESA project with instruments funded by ESA Member States (especially the PI countries: France, Germany, The Netherlands and the UK) and with the participation of ISAS and NASA.

Table 1. Observed sources and their properties.

Source	RA (2000)	Dec (2000)	Observation ID[a]	15 μm Flux[b] (Jy)	Luminosity (10^5 $L_\odot$)	Distance (kpc)	Reference[c]
AFGL 2591	$20^h29^m24\overset{s}{.}7$	$+40°11'19''$	02899582	790	0.2	1	1, 1
			14200503				
			19301928				
AFGL 2136	$18^h22^m26\overset{s}{.}3$	$-13°30'08''$	12000925	260	0.7	2	1, 1
			12800302				
AFGL 4176	$13^h43^m02\overset{s}{.}1$	$-62°08'52''$	11701404	400	1.8	4	2, 3
			30601344				
MonR2 IRS3	$06^h07^m48\overset{s}{.}2$	$-06°22'55''$	71101802	540	0.13	0.95	4, 5
NGC 7538 IRS 1	$23^h13^m45\overset{s}{.}4$	$+61°28'09''$	28301235	420	1.3	2.8	1, 1
NGC 7538 IRS 9	$23^h14^m01\overset{s}{.}6$	$+61°27'20''$	09801533	110	0.4	2.8	1, 1
NGC 2024 IRS 2	$05^h41^m45\overset{s}{.}8$	$-01°54'34''$	66701228	40	1	0.4	6, 7
AFGL 2059	$18^h04^m53\overset{s}{.}0$	$-24°26'45''$	49302585	160	0.16	1.5	2, 3
G 333.3–0.4	$16^h21^m30\overset{s}{.}9$	$-50°25'07''$	45800340	190	6	3.9	2, 8
NGC 3576	$11^h11^m53\overset{s}{.}9$	$-61°18'25''$	29200143	380	3.5	2.4	2, 9
S 140 IRS 1	$22^h19^m18\overset{s}{.}2$	$+63°18'47''$	26301731	630	0.2	0.9	1, 1
W 33 A	$18^h14^m39\overset{s}{.}4$	$-17°52'01''$	12501301	50	1.0	4	1, 1
			12501406				
			32900920				
			33201806				
			46700521				
			46700801				
W 3 IRS 4	$02^h25^m30\overset{s}{.}9$	$+62°06'21''$	61601103	140	1–2	2.2	10, 1
W 3 IRS 5	$02^h25^m40\overset{s}{.}9$	$+62°05'52''$	42701224	860	1.7	2.2	1, 1

[a] For sources where multiple IDs are listed, the spectra presented in this paper are a combination of all of these.
[b] Continuum flux at ~15 μm in the ISO-SWS aperture, obtained by extrapolating the continuum flux in the 14.5–14.8 μm region.
[c] The first reference refers to the luminosity, the second to the distance.
References: 1. van der Tak et al. (2000b); 2. Lahuis & van Dishoeck (2000); 3. Henning et al. (1990); 4. Henning et al. (1992); 5. Giannakopoulou et al. (1997); 6. Thompson et al. (1981); 7. Anthony-Twarog (1982); 8. Azcarate et al. (1986); 9. Persi et al. (1987); 10. Helmich et al. (1994).

chemistry in warmer sources (van Dishoeck 1998). One of the main questions is whether abundances of gas-phase CO_2 as high as $\sim 10^{-5}$ are observed in any star-forming region.

In this paper, observations of the ν_2 ro-vibrational band of gas-phase CO_2 around 15 μm toward 14 embedded massive young stars are presented. All sources in our sample have luminosities between $\sim 10^4$–10^5 $L_\odot$ and do have complementary ISO data on ices and other gas-phase molecules (e.g. Lahuis & van Dishoeck 2000; Gerakines et al. 1999; Keane et al. 2001b). The observations and reduction of the data are summarized in Sect. 2. Section 3 describes the analysis, using pure absorption models to derive abundances and gas/solid ratios. Radiative transfer effects are taken into account in Sect. 4 and the results are discussed in Sect. 5. Finally, the conclusions are presented in Sect. 6.

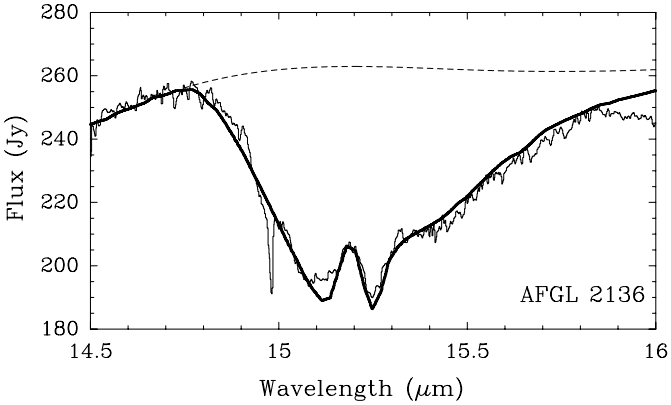

Fig. 1. ISO-SWS spectrum of AFGL 2136 between 14.5 and 16 μm. The dashed line shows the adopted continuum, the solid line a good fitting ice mixture of polar + annealed ice (H_2O:CO:CO_2 = 100:3:20+ H_2O:CH_3OH:CO_2 = 1:1:1 respectively) to the observed CO_2 ice band (Gerakines et al. 1999).

2. Observations and reduction

The ν_2 ro-vibrational band of gas-phase CO_2 around 15 μm has been observed with the Short Wavelength Spectrometer (SWS) in the AOT6 grating mode toward all sources. The spectra have been reduced using the ISO-SWS Interactive Analysis System `SIA` using the ISO Off-line Processing (OLP version 10) software modules and calibration files. In addition, the instrumental fringes have been removed by a combination of an optimized spectral response calibration and robust sine wave fitting (Lahuis & van Dishoeck 2000). The spectra have been rebinned to an effective spectral resolution of

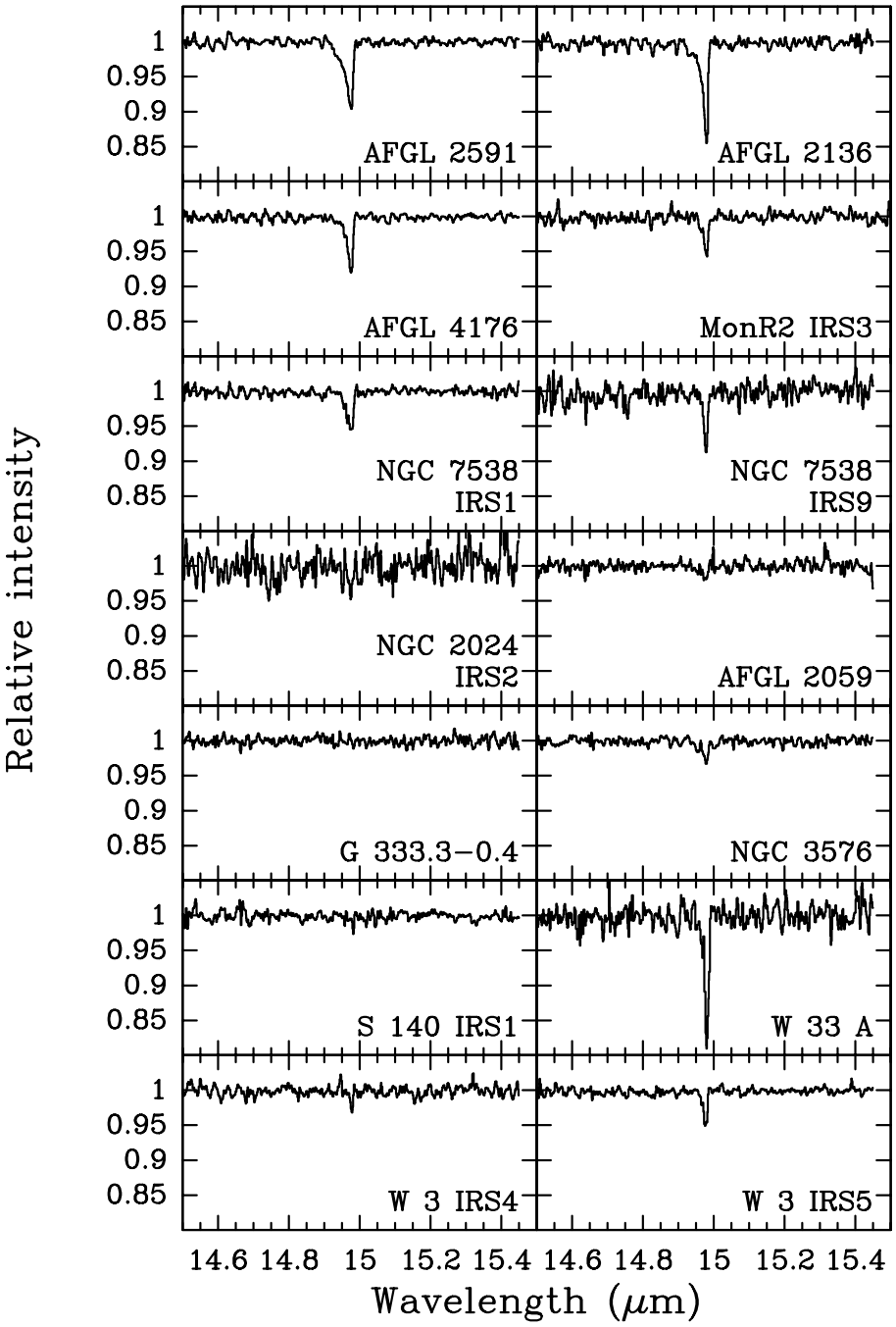

Fig. 2. Normalised ISO-SWS spectra in the region of the gas-phase CO_2 ν_2 bending mode for all sources. The solid CO_2 feature has been removed (see text).

$\Delta\lambda = 0.0085\ \mu$m. The S/N ratio on the continuum is typically 50–100 in the final spectra.

The ν_2 ro-vibrational band of gas-phase CO_2 has been detected toward the sources AFGL 2136, AFGL 2591, AFGL 4176, MonR2 IRS3, NGC 7538 IRS1, NGC 7538 IRS9, W 33 A, and W 3 IRS5. The spectra of AFGL 2136, AFGL 2591, AFGL 4176, and NGC 7538 IRS9 have been analysed previously by van Dishoeck et al. (1996). The reduced spectra presented here are however of much higher quality. Both the instrument calibration and the reduction routines within the ISO-SWS pipeline as well as the SWS Interactive Analysis have improved significantly since 1996. In addition for AFGL 2136, AFGL 2591, and AFGL 4176, the spectra of multiple independent observations of the same source have been combined, leading to an additional increase in the final S/N ratio.

An example of the resulting spectra is shown in Fig. 1 together with a fit to the CO_2 ice band, using an ice mixture similar to that found by Gerakines et al. (1999). Although the laboratory ice fit follows the solid-state feature quite well, it shows some small deficiencies, which could be due to the presence of other solid-state features that are not accounted for in the

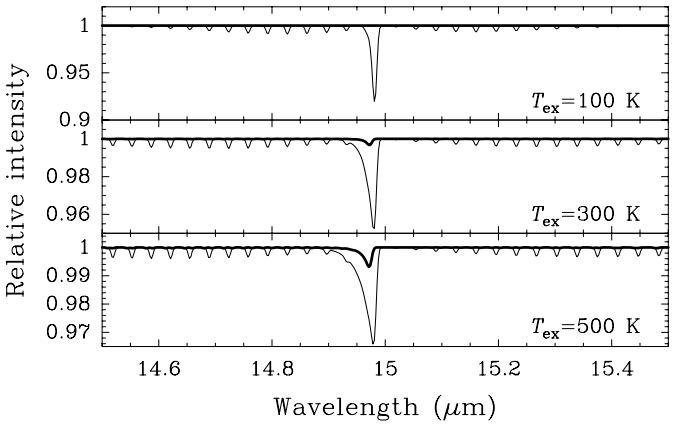

Fig. 3. The strength of the CO_2 (02^20) ← (01^10) hotband (thick line) compared to the fundamental (01^10) ← (00^00) band (thin line) for different excitation temperatures, using b = 3 km s^{-1} and $N = 1 \times 10^{16}$ cm^{-2}.

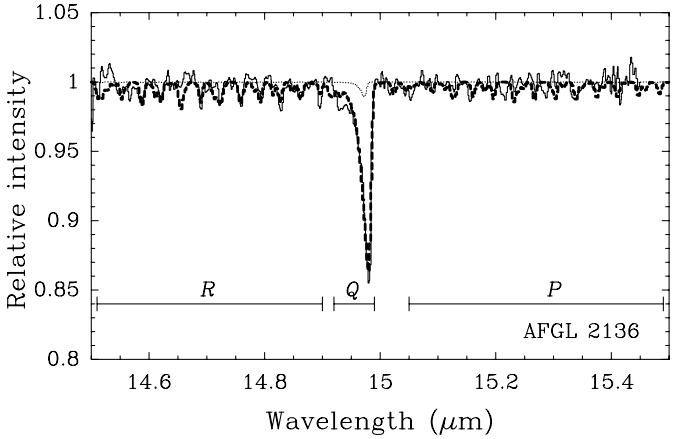

Fig. 4. Example of a good fitting model for the observed CO_2 spectrum toward AFGL 2136, using the best fit parameters from Table 2 (dashed line). The dotted line shows the contribution of the (02^20) ← (01^10) hotband. The solid line is the observed ISO-SWS spectrum divided by the continuum. The P, Q, and R-branches of the CO_2 ν_2 ro-vibrational band are indicated.

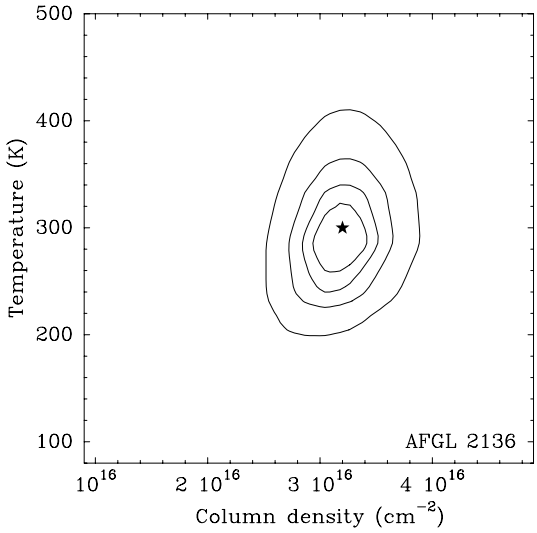

Fig. 5. Example of the χ^2 distribution for AFGL 2136. The star indicates the minimum χ^2 and the contours are 2.5, 5, 10, and 22.5% above the minimum χ^2. The latter contour roughly corresponds to a 3σ deviation of the model from the observed CO_2 band for this source.

ice fit. Therefore the final spectra have been divided by a manual fit to the CO_2 ice band, resulting in the normalised spectra presented in Fig. 2. Different fits to the continuum have been made to investigate their effect on the shape and depth of the gas-phase CO_2 band and these have been taken into account in the analysis of the spectra.

3. Analysis

3.1. Homogeneous pure absorption models

The modeling of the spectra has been performed by computing synthetic spectra using the method described in Lahuis & van Dishoeck (2000). In this method, the source is assumed to be a homogeneous sphere with a single temperature T_{ex} and column density N. Here it is assumed that only absorption takes place and that emission can be neglected. The effects of adopting a non-homogeneous source and including emission are discussed in Sect. 4. The models are not sensitive to the CO_2 line width as long as the lines are not saturated, which becomes important only for $b \lesssim 1$ km s^{-1}. A mean Doppler b-value of 3 km s^{-1} is adopted (see also Boonman et al. 2003), but values up to b = 10 km s^{-1} have been explored. Similar values are used in the modeling of other observed ro-vibrational absorption lines in the same wavelength region toward these sources (e.g. Lahuis & van Dishoeck 2000; Keane et al. 2001a). For comparison, Mitchell et al. (1990) derive line widths of $b \sim 4$–7 km s^{-1} from high-resolution observations of the CO ro-vibrational band around 4.7 μm. The resulting synthetic spectra have been convolved to the nominal spectral resolution of the ISO-SWS spectra for comparison with the data.

The molecular line data have been taken from the HITRAN 2000 database (`http://www.hitran.com`). The model includes the fundamental (01^10) ← (00^00) band at 14.983 μm, the hotbands (02^20) ← (01^10) and (02^00) ← (01^10) at 14.976 and 16.18 μm respectively, and the (10^00) ← (01^10) band at 13.87 μm. The (02^00) ← (01^10) and (10^00) ← (01^10) bands are not detected. The (02^20) ← (01^10) hotband coincides with the fundamental Q-branch, making it difficult to detect. Figure 3 shows the shape and strength of the CO_2 fundamental and the (02^20) ← (01^10) hotband for different excitation temperatures. This shows that for $T_{ex} \gtrsim 300$ K the (02^20) ← (01^10) hotband starts to play a role. This hotband was not included in the previous modeling of the CO_2 spectra by van Dishoeck et al. (1996).

The best fit to the data has been determined using the reduced χ^2_ν-method. Since the P-branches of the C_2H_2 ν_5 and HCN ν_2 ro-vibrational bands extend into the region of the CO_2 ν_2 band, these bands are included in the modeling, using the best fit parameters from Lahuis & van Dishoeck (2000). For all sources, their contribution is less than the noise level, but they are included for consistency. The best fitting model parameters are listed in Table 2 for all sources. The uncertainty in the excitation temperature includes errors due to different continuum fits.

Table 2. Model parameters for the ν_2 band of CO_2.

Source	$T_{ex}(CO_2)$ K	$N(CO_2)$ 10^{16} cm^{-2}	$N(H_2)^a$ 10^{22} cm^{-2}	$x(CO_2)^b$ 10^{-7}
AFGL 2591	550^{+100}_{-100}	2.6 ± 0.5	9.6	2.7
AFGL 2136	300^{+100}_{-100}	3.2 ± 0.7	11.	2.9
AFGL 4176	450^{+250}_{-150}	1.7 ± 0.5	8.0	2.1
MonR2 IRS3	225^{+125}_{-100}	1.0 ± 0.3	4.9[c]	2.0
NGC 7538 IRS1	450^{+175}_{-175}	1.3 ± 0.4	8.6	1.5
NGC 7538 IRS9	200^{+125}_{-100}	1.4 ± 0.6	4.9	2.9
NGC 2024 IRS2[d]	45	<1.0	3.5	<2.9
AFGL 2059	500[e]	<0.8	4	<2.0
G 333.3-0.4	300[f]	<0.5	15	<0.3
NGC 3576	500[ef]	<0.8	8	<1.0
S 140 IRS1	390[g]	<0.8	3.7	<2.2
W 33 A	100^{+50}_{-30}	3.2 ± 1.0	13.	2.5
W 3 IRS4[h]	55	<0.5	11.	<0.5
W 3 IRS5	250^{+125}_{-100}	0.9 ± 0.2	13.	0.7
Orion BN/KL[i]	220^{+55}_{-40}	6.0 ± 1.2	8–30	1.6–8.9

[a] From Lahuis & van Dishoeck (2000), unless otherwise noted.
[b] $N(CO_2)/N(H_2)$.
[c] Using $N(^{13}CO)$ from Giannakopoulou et al. (1997).
[d] Using $T_{ex}(^{12}CO)$ and $N(H_2)$ from Lacy et al. (1994).
[e] $T_{ex}(H_2O)$ from Boonman et al. (2000).
[f] $T_{ex}(C_2H_2)$ from Lahuis & van Dishoeck (2000).
[g] $T_{ex}(^{13}CO)$ from Mitchell et al. (1990).
[h] Using T_{kin} and $N(CO)$ from Helmich & van Dishoeck (1997).
[i] From Boonman et al. (2003).

The results show that warm CO_2 gas at $T \geq 200$ K is detected toward half of the sources and suggest that for the hottest sources, AFGL 2591, AFGL 2136, and AFGL 4176, also the $(02^20) \leftarrow (01^10)$ hotband contributes. The gas-phase $^{13}CO_2$ band near 15.4 μm is not detected in our sources.

A good fitting CO_2 model is presented in Fig. 4. Figure 5 shows an example of χ^2_ν contours for the source AFGL 2136. It illustrates that the column density of the gas-phase CO_2 is well constrained, but that the excitation temperature shows a larger spread.

Comparison of our results for AFGL 2136 to those by Sandford et al. (2001) shows a lower excitation temperature than their T_{ex} of 580 K. Also, their column density in the 580 K gas is more than an order of magnitude higher than that found here. This discrepancy is likely caused by the low signal-to-noise in the spectrum presented by Sandford et al. (2001), which is also hampered by the presence of instrumental fringes. These fringes are carefully removed in our spectra. In addition, our AFGL 2136 spectrum shows the detection of a few *P*- and *R*-branch lines (Fig. 4), which poses an extra constraint on the excitation temperature and column density. The fact that the CO_2 ice fit shown in Fig. 1 does not match the observed continuum very well between 14.6 and 14.8 μm introduces an uncertainty of ~100 K in the excitation temperature, which is accounted for in the results in Table 2. Therefore, the newly reduced spectra presented here allow a more reliable estimate of the excitation temperature and column density of the CO_2 ν_2 ro-vibrational band.

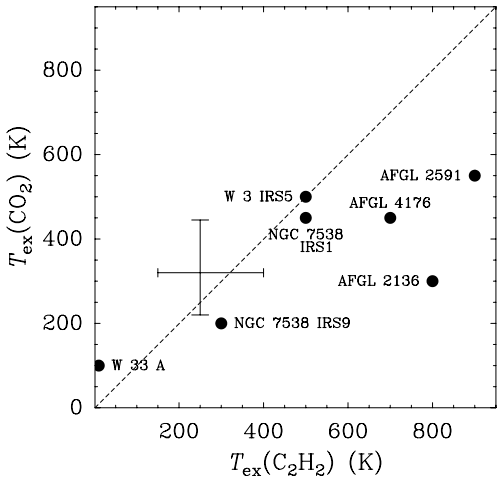

Fig. 6. Correlation between the CO_2 excitation temperature $T_{ex}(CO_2)$ and that of C_2H_2, a good tracer of the warm gas (Lahuis & van Dishoeck 2000). Only those sources are shown for which both excitation temperatures are determined. The cross denotes typical error bars for $T_{ex} \gtrsim 200$ K.

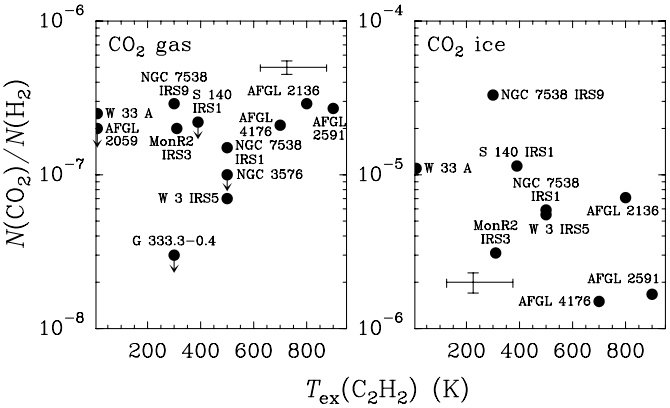

Fig. 7. The CO_2 gas-phase abundances from Table 2 (left panel) and the CO_2 ice abundances from Gerakines et al. (1999) (right panel) versus $T_{ex}(C_2H_2)$ from Lahuis & van Dishoeck (2000). The crosses denote typical error bars for $T_{ex} \gtrsim 200$ K. For MonR2 IRS3 and S 140 IRS1 the ^{13}CO temperatures from Giannakopoulou et al. (1997) and Mitchell et al. (1990) respectively, are plotted.

Figure 6 presents a comparison of the CO_2 excitation temperature $T_{ex}(CO_2)$ and that of C_2H_2, a good tracer of the warm gas (Lahuis & van Dishoeck 2000). It is seen that $T_{ex}(CO_2)$ increases with $T_{ex}(C_2H_2)$, indicating that CO_2 also traces warm gas. However, the increase is not as strong as for C_2H_2 (Fig. 6). Note that for NGC 7538 IRS1 a C_2H_2 excitation temperature of ~500 K is found from a new, updated reduction of the spectra, much lower than the $T_{ex}(C_2H_2) = 800$ K listed in Lahuis & van Dishoeck (2000).

3.2. Abundances

The CO_2 column densities have been converted into abundances, using the total H_2 column densities (cold + warm

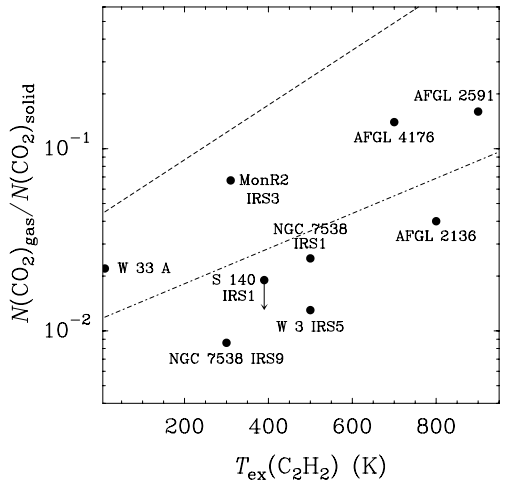

Fig. 8. Gas/solid ratio for CO_2 versus $T_{ex}(C_2H_2)$ (filled circles). For MonR2 IRS3 and S 140 IRS1, $T_{ex}(^{13}CO)$ is used (Giannakopoulou et al. 1997; Mitchell et al. 1990). The dot-dashed line shows the least-squares fit to the CO_2 gas/solid ratios and the dashed line the least-squares fit to the H_2O gas/solid ratios from Boonman & van Dishoeck (2003).

components) derived from infrared observations of ^{13}CO (e.g. Mitchell et al. 1990). A $^{12}CO/^{13}CO$ ratio of 60 and a $^{12}CO/H_2$ ratio of 2×10^{-4} have been assumed (Lahuis & van Dishoeck 2000; Lacy et al. 1994). Typical derived CO_2 abundances are a few $\times 10^{-7}$ (Table 2). The inferred abundances do not show a clear trend with temperature (Fig. 7). Using the H_2 column densities in the warm gas only increases the gas-phase CO_2 abundance by a factor of ∼2 for most sources, but does not change the lack of a trend with temperature. The abundances differ by less than a factor of ∼4 between the sources, except for G 333.3-0.4 (Fig. 7). However, for G 333.3-0.4 the H_2 column density is determined from the $C^{17}O$ J = 2–1 submillimeter transition, resulting in an upper limit on the H_2 column density, and consequently a rather uncertain CO_2 abundance.

The derived CO_2 abundances for AFGL 2591, AFGL 2136, and AFGL 4176 are a factor of ∼2.5–4 higher than the tentative values from van Dishoeck et al. (1996). For NGC 7538 IRS9 the tentative value falls within the error bars of the CO_2 abundance derived here. The inferred CO_2 abundances agree well with the abundance range found toward Orion IRc2/BN (Table 2).

3.3. Gas/solid ratios

Gas/solid ratios can be determined by combining the derived gas-phase CO_2 column densities with those for CO_2 ice for the same sources from Gerakines et al. (1999) (see Fig. 7). This ratio increases with temperature, consistent with the location of CO_2 in the warm inner part of the envelope, above the evaporation temperature (Fig. 8). However, the increase is less strong and the ratios are lower than for H_2O, although pure CO_2 ice is more volatile than H_2O (Fig. 8; Boonman & van Dishoeck 2003). This is probably due to the fact that toward our sources CO_2 ice is mostly embedded in a H_2O ice matrix and that its column density is only 10–23% of that of H_2O ice (Gerakines et al. 1999). In addition, gas-phase H_2O abundances of up to $\sim 10^{-4}$ are easily formed above $T > 230$–300 K, thus rapidly increasing the H_2O gas/solid ratios (Charnley 1997).

4. Radiative transfer effects

4.1. Filling in by emission

In this section, the effect of possible emission along the line of sight on the derived CO_2 column densities and abundances is investigated. To this purpose a similar excitation model as that described in Boonman et al. (2003) has been set-up. This excitation model includes energy levels for CO_2 up to $J = 40$ in both the $\nu_2 = 0$ and 1 vibrational states. The level populations are calculated adopting a Boltzmann distribution using T_{ex} from Table 2. As a central radiation source, a blackbody with $T = 300$ to 600 K has been explored.

Adopting a homogeneous source as before, but including both absorption and emission along the line of sight, shows that the CO_2 column densities needed to match the observations are up to ∼30% higher than those listed in Table 2 as long as the excitation temperature is less than ∼250–300 K. This is within the listed error bars. The emission only becomes important for $T_{ex} \gtrsim 250$–300 K, i.e. for the sources W 3 IRS5, AFGL 2136, AFGL 4176, NGC 7538 IRS1, and AFGL 2591 (see also Boonman et al. 2003). For these sources, the CO_2 column density that best matches the observations can be up to a factor of ∼3 higher than that derived from the pure absorption models (Table 2). Note that this model does not include other radiative transfer effects, such as infrared pumping, nor does it include temperature and density gradients, so that the derived CO_2 abundances within this model are not very accurate.

4.2. Temperature and density gradients: Jump models

Van der Tak et al. (2000b) show that a density and temperature gradient is present in their sample of deeply embedded massive young stars, which is a sub-set of the sample studied here. Since radiative transfer effects are expected to be largest for the warmer sources, AFGL 2591 is taken as a test case. Adopting the physical model for AFGL 2591 derived by van der Tak et al. (2000b), the level populations and radiative transfer are calculated with the Monte Carlo code of Hogerheijde & van der Tak (2000) on a grid of concentric shells, assuming spherical geometry. The calculations include energy levels up to $J = 40$ in both the $\nu_2 = 0$ and $\nu_2 = 1$ states, the same as in the excitation model described in Sect. 4.1. The collisional rate coefficients used are taken from Allen et al. (1980). Radiative excitation through the 15 μm band due to warm dust mixed with the gas is included, using grain opacities from Ossenkopf & Henning (1994) and assuming $T_{dust} = T_{gas}$. No external radiation field apart from the 2.73 K cosmic background radiation was applied. The resulting level populations are used in the excitation model described above to calculate a synthetic model spectrum including both emission and absorption along the line of sight. As a central radiation source a blackbody at $T > T_{dust}$ in the innermost shell is chosen. The resulting model spectrum is then compared with the observed absorption spectrum.

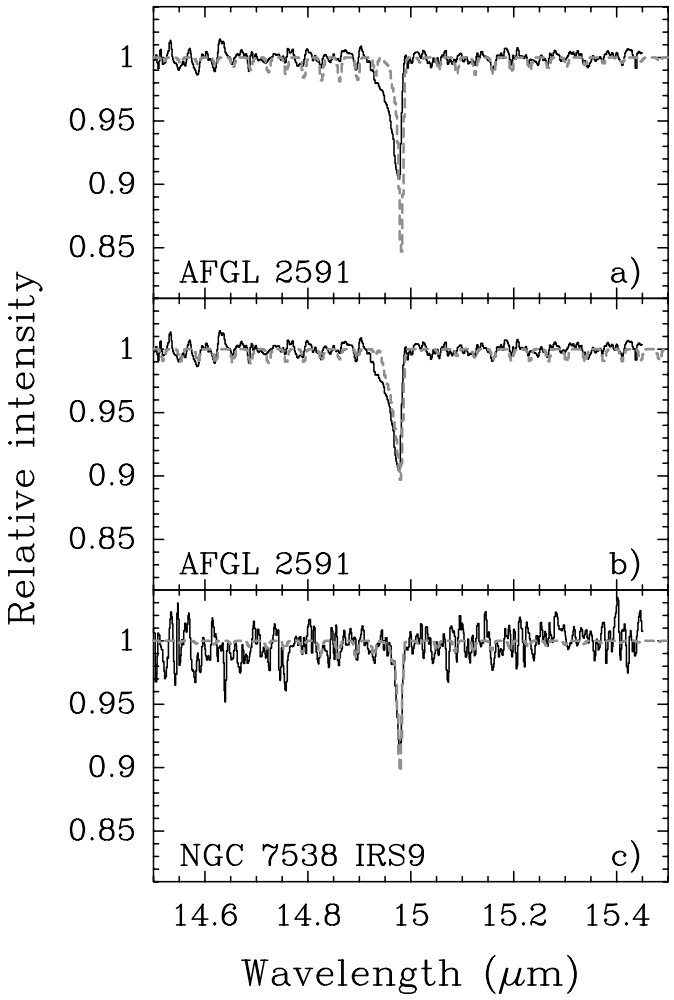

Fig. 9. Results from the detailed radiative transfer models including temperature and density gradients (see Sect. 4.2). The solid line shows the data, the dashed line the model spectrum. **a)** Model spectrum for AFGL 2591 using a constant CO_2 abundance of $n(CO_2)/n(H_2) = 3 \times 10^{-7}$ throughout the envelope, similar to that inferred from the pure absorption models in Sect. 3.2. **b)** Model spectrum for AFGL 2591 using $n(CO_2)/n(H_2) = 2 \times 10^{-6}$ for $T > 300$ K and $n(CO_2)/n(H_2) = 1 \times 10^{-8}$ for $T < 300$ K. **c)** Model spectrum for NGC 7538 IRS9 using a constant CO_2 abundance of $n(CO_2)/n(H_2) = 7 \times 10^{-8}$.

For AFGL 2591 it is found that a constant CO_2 abundance $x(CO_2) = n(CO_2)/n(H_2)$ throughout the envelope produces a synthetic spectrum with a Q-branch that is too narrow compared to the observations (Fig. 9). This indicates that the constant abundance model is dominated by absorption from gas at $T < 300$ K. Therefore a model with a jump in the abundance at $T = 300$ K has been tried. It is found that a model spectrum with a CO_2 abundance of ~ 1–2×10^{-6} for $T > 300$ K and 10^{-8} for $T < 300$ K can reasonably explain the observed spectrum (Fig. 9). Applying a jump at lower temperatures, e.g. at $T = 200$ K or $T = 100$ K produces a Q-branch that is too narrow. This indicates that the observed Q-branch represents warm CO_2 gas from the inner part of the molecular envelope at $T \geq 300$ K, in agreement with that inferred from the pure absorption models. It also shows that the CO_2 abundance in the outer envelope is much lower, about two orders of magnitude. Similar jumps in the abundance have been seen for other molecules toward AFGL 2591, such as HCN, H_2O, and SO_2 (Boonman et al. 2001; Boonman & van Dishoeck 2003; Keane et al. 2001a; van der Tak et al. 2003).

Similarly one of the colder sources, NGC 7538 IRS9, is modeled for comparison using the physical model derived by van der Tak et al. (2000b). It is found that a constant CO_2 abundance of $\sim 7 \times 10^{-8}$ can reproduce the observed spectrum. A model with a jump in the abundance at $T = 100$ K and $x(CO_2) = 2 \times 10^{-7}$ for $T > 100$ K and $x(CO_2) = 1 \times 10^{-9}$ for $T < 100$ K gives a similarly good fit in terms of χ^2. This indicates that for NGC 7538 IRS9 no evidence for a jump in the abundance at temperatures $T \geq 300$ K is found. The result that a jump in the abundance at $T = 100$ K fits the observed spectrum equally well as the constant abundance model may suggest that most of the CO_2 is frozen-out onto the grains below this temperature.

The corresponding CO_2 column densities for the best fit models for AFGL 2591 and NGC 7538 IRS9 are a factor of ~2–4 and ~1.5–2 higher than those listed in Table 2 respectively. On the other hand, the abundance toward NGC 7538 IRS9 is somewhat lower than that derived from the pure absorption models (Table 2).

The above results indicate that a jump in the CO_2 abundance is present for the warmer, more evolved sources, but that no such jump is seen toward the colder objects. This suggests that also for AFGL 2136, AFGL 4176, and NGC 7538 IRS1 a jump in the CO_2 abundance is present.

Observations of the intermediate-mass protostars AFGL 490 and AFGL 7009S show CO_2 abundances of a few $\times 10^{-7}$, similar to those derived from the pure absorption models in Sect. 3.2 (Schreyer et al. 2002; Dartois et al. 1998). These CO_2 abundances do not show a clear trend with temperature (Fig. 7). However the results from the detailed radiative transfer models indicate much higher CO_2 abundances in the warm inner part of the envelope for the more evolved sources. Combined with the somewhat lower CO_2 abundance toward the cold source NGC 7538 IRS9, this suggests that the CO_2 abundance increases with temperature and evolutionary state.

5. Discussion

5.1. CO_2 as an evolutionary tracer

In Sect. 3 it is shown that $T_{ex}(CO_2)$ increases with $T_{ex}(C_2H_2)$, indicating that it is a tracer of the warm gas. The gas/solid ratio also increases with the temperature of the warm gas and the CO_2 ice abundance decreases (Figs. 7 and 8). The higher ratios for the warmer sources suggest that they are in a later evolutionary stage than the sources with low gas/solid ratios, with the higher temperatures due to dispersion of a larger fraction of the molecular envelope (van der Tak et al. 2000b; van Dishoeck & van der Tak 2000).

Although the abundances derived from the pure absorption models do not show a clear trend with temperature, the results from the jump models in Sect. 4.2 suggest that the CO_2 abundance increases with temperature. In addition, the same sources with a high CO_2 excitation temperature and correspondingly a

higher gas/solid ratio also show evidence for thermal processing of $^{13}CO_2$ and CO_2 ice (Boogert et al. 2000; Gerakines et al. 1999). Together, this shows that CO_2 can be used as an evolutionary tracer.

5.2. Chemistry in cold sources: NGC 7538 IRS9

Envelope models by Doty et al. (2002) predict gas-phase CO_2 abundances of a $\sim 10^{-7}$–10^{-6} at $T \lesssim 300$ K for $t \sim 3 \times 10^3$–10^5 yrs. This indicates that pure gas-phase chemistry can explain the observed abundances toward the colder sources, such as NGC 7538 IRS9, that show no evidence for a jump in the abundance for $T \gtrsim 300$ K (Sect. 4.2).

In the colder sources, the high CO_2 ice abundances and low gas/solid ratios indicate that a large fraction of the envelope still contains cold material. This suggests that the observed gas-phase CO_2 absorption is dominated by the colder outer envelope where evaporation has not yet taken place. However, these sources may still hide a small region in the inner envelope containing hot, abundant gas-phase CO_2, which cannot be detected with the present observations, e.g. due to continuum optical depth effects.

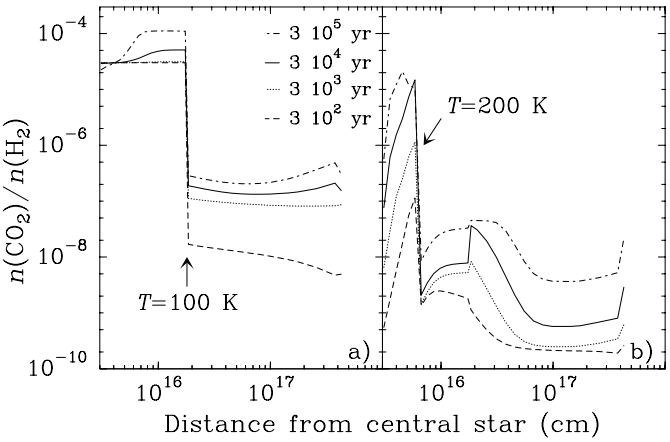

Fig. 10. Gas-phase CO_2 abundances in the envelope of AFGL 2591 for chemical ages of 3×10^2, 3×10^3, 3×10^4, and 3×10^5 yrs (after Doty et al. 2002). **a)** Gas-phase chemistry including evaporation of CO_2 ice for $T \sim 100$ K. The initial CO_2 abundance of 3×10^{-5} for $T \gtrsim 100$ K and the cosmic ray ionization rate of $\zeta_{CR} = 5.6 \times 10^{-17}$ s^{-1} from Doty et al. (2002) have been adopted. **b)** Gas-phase chemistry adopting $n(CO_2)/n(H_2) = 0$ initially, $\zeta_{CR} \sim 10^{-20}$ s^{-1} for $T < 200$ K, and an ionization rate of $\zeta = 2 \times 10^{-16}$ s^{-1} for $T > 200$ K.

5.3. Chemistry in warm sources: AFGL 2591

5.3.1. Comparison to hot core and shock models

The high inferred gas-phase CO_2 abundance in the inner envelope of AFGL 2591 for $T > 300$ K but lack of a jump at $T \sim 100$ K in Sect. 4.2 is unexpected. Such a jump is observed for simple ice constituents such as H_2O and CH_3OH in hot-core type objects (e.g. van der Tak et al. 2000a; Maret et al. 2002), which is due to evaporation of H_2O-rich ices around $T \sim 90$–110 K (Fraser et al. 2001). Since most of the CO_2 ice is embedded in H_2O ice, it will evaporate around the same temperature (Fig. 10). The high gas/solid ratio and low CO_2 ice abundance of 1.7×10^{-6} (Gerakines et al. 1999) toward AFGL 2591 indicate that evaporation of CO_2 ice does occur (see also Fig. 7, right panel). The lack of a jump around 100 K then indicates that CO_2 must be rapidly destroyed in the gas phase after evaporation in the $T \sim 100$–300 K zone. At $T > 300$ K, either the CO_2 is only partially destroyed or it has quickly reformed in the gas-phase.

Second, the CO_2 solid-state abundances toward the cold sources with little or no ice evaporation are an order of magnitude higher than the gas-phase CO_2 abundance in the inner hot envelope of AFGL 2591 (Fig. 7). This suggests that CO_2 is originally formed on grain surfaces, and not simply due to freeze-out of CO_2 gas. The discrepancy between the observed gas-phase and solid-state CO_2 abundances provides further evidence for rapid destruction of CO_2 in the gas-phase after evaporation from the grains. Charnley & Kaufman (2000) propose that shocks can be responsible for this.

A study of the Orion shocked regions Peak 1 and 2 shows gas-phase CO_2 abundances of ~ 0.3–6×10^{-8}, which are best explained by destruction of the CO_2 in a shock containing a high H/H_2 ratio of ~ 0.01, and subsequent reformation in the gas-phase (Boonman et al. 2003). A similar abundance of $\sim 10^{-8}$ is found in the envelope of AFGL 2591 for $T < 300$ K in Sect. 4.2. This suggests that the outflow may have (partially) destroyed the CO_2 in the envelope of AFGL 2591 in the past, and that it has not yet been reformed. However, such a shock model cannot explain the high abundance in the inner envelope at $T > 300$ K, unless destruction is much less efficient in the densest inner part due to e.g. a lower H/H_2 ratio.

Doty et al. (2002) propose that a heating event can also destroy CO_2 through the reaction $CO_2 + H_2 \rightarrow CO + H_2O$. Recent calculations by Talbi & Herbst (2002) however show that this reaction is not likely to play a dominant role in the interstellar medium.

The primary formation route of CO_2 in the gas-phase is through the reaction $CO + OH \rightarrow CO_2 + H$ which proceeds rapidly at $T \geq 100$ K (Charnley 1997). Above $T \sim 230$–300 K most of the OH is driven into H_2O, thus reducing the formation of CO_2 through gas-phase reactions. This formation route predicts gas-phase CO_2 abundances of $\sim 10^{-6}$ at $T = 100$ K to a few $\times 10^{-7}$ at $T = 300$ K (Charnley 1997). This is much lower than the inferred CO_2 abundance of 1–2×10^{-6} for $T > 300$ K toward AFGL 2591. On the other hand, gas-phase CO_2 can also be formed through the reaction of $CO + H_2O$, but this reaction has an energy barrier of $\sim 5.2 \times 10^4$ K, preventing production of significant CO_2 in the molecular envelope.

5.3.2. Comparison to UV, cosmic- and X-ray models

Alternatively, the UV flux from the protostar may be high enough in the inner envelope to produce OH through direct photodissociation of H_2O. This could maintain sufficient OH in the gas-phase to form abundant gas-phase CO_2 in the interior at $T \gtrsim 300$ K. However, photodissociation is estimated to play a role only up to $r \sim 10^{14}$ cm from the central source, much smaller than the inner radius of the physical model used

in Sect. 4.2. Doty et al. (2002) suggest that cosmic-ray or X-ray ionization can also produce significant OH, which is then channelled into CO_2. Using the chemical model from Doty et al. (2002) for AFGL 2591 and adopting a zero initial gas-phase CO_2 abundance corresponding to the destruction of CO_2 by a shock, indeed predicts enhanced CO_2 abundances of $\sim 10^{-6}$–10^{-5} in the interior for $T > 200$ K if a high ionization rate of 2×10^{-16} s^{-1} is adopted (Fig. 10). This illustrates that a high ionization rate in the inner envelope can produce a jump in the CO_2 abundance at temperatures larger than 100 K as found for AFGL 2591. This model adopts an artificially low cosmic-ray ionization rate of $\zeta_{\rm CR} \sim 10^{-20}$ s^{-1} in the outer envelope, predicting gas-phase CO_2 abundances of $\sim 10^{-8}$ for $T \lesssim 200$ K, consistent with that found in Sect. 4.2. Adopting $\zeta_{\rm CR} = 5.6 \times 1^{-17}$ s^{-1} as derived by van der Tak & van Dishoeck (2000) from HCO^+ observations results in much higher abundances of $\sim 10^{-6}$–10^{-5} for $T \sim 100$–200 K and $\sim 10^{-7}$ for $T < 100$ K, somewhat higher than that found for AFGL 2591. However, freeze-out of CO_2 onto the grains is likely to play a role for $T < 100$ K, which is not included in the model.

Doty et al. (2002) note that the ionization rate needs to be at least on the order of $\zeta = 5.6 \times 10^{-17}$ s^{-1} in the interior, in order to account for the high gas-phase HCN abundances for $T \gtrsim 300$ K. This is consistent with our proposed chemical scenario of a high ionization rate in the inner envelope, explaining the jump in the CO_2 abundance for $T \gtrsim 300$ K. Although the production of CO_2 through X-ray ionization involves destruction of gas-phase H_2O and CO, the predicted enhanced CO_2 abundances in Fig. 10 are $\lesssim$10% of those predicted for H_2O and CO. In addition, abundant gas-phase H_2O and CO are observed in the warm inner envelope from infrared absorption (e.g. Boonman et al. 2000; Mitchell et al. 1990), suggesting that these molecules are not significantly affected by X-rays. Since the cosmic-ray ionization rate is expected to be roughly constant or potentially decreases inward within the molecular envelope, the enhanced ionization rate in the warm interior seems more likely caused by X-rays from the young star than cosmic rays from outside the molecular envelope. Using the photoionization cross section from Wilms et al. (2000), it is estimated that X-rays of a few keV can affect the chemistry up to radii at which $T \sim 400$ K in the envelopes of massive protostars. Recently, X-ray emission within this energy range has been detected toward MonR2 IRS3, one of our warm sources, further suggesting that X-ray ionization may be important for the CO_2 chemistry in the inner envelope of massive young stars (Preibisch et al. 2002; Kohno et al. 2002).

5.3.3. Comparison to dynamical models

Another possibility is that gas-phase CO_2 in the interior results from ice evaporation at $T \sim 100$ K in the past, and is subsequently heated as the protostar evolves to higher temperatures at the same point in the envelope, without being destroyed. However, material initially at $T < 100$ K will consequently be heated to $T > 100$ K, where ice evaporation occurs almost instantaneously (Fraser et al. 2001). This predicts gas-phase CO_2 abundances of $\sim 10^{-6}$–10^{-5} between 100 and 300 K, contrary to the inferred abundance of $\sim 10^{-8}$.

A second scenario to consider would be the dynamical transport of gas-phase CO_2 formed between 100 and 300 K inward to the $T > 300$ K region, e.g. through infall motions. In this case, however, the CO_2-ice containing material at $T < 100$ K would be transported inward to the $T = 100$–300 K region. At this point, the CO_2 ice would evaporate immediately, thus maintaining a large gas-phase CO_2 abundance for $T = 100$–300 K.

At present, a combination of the destruction of CO_2 by a past shock in the outflow, and either a high X-ray ionization rate in the interior which rapidly reforms gas-phase CO_2 for $T > 300$ K or incomplete destruction of evaporated CO_2 for $T > 300$ K, seems the most likely explanation for the inferred jump in the gas-phase CO_2 abundance for $T > 300$ K toward AFGL 2591. As noted by Doty et al. (2002), more experimental work on the chemistry of gas-phase CO_2 is needed to obtain a better knowledge of the formation and/or destruction pathways of gas-phase CO_2 in the envelopes of massive protostars.

6. Conclusions

The main conclusions of this work are:

- The CO_2 excitation temperature correlates well with that of C_2H_2, a good tracer of the warm gas.
- Overall abundances of a few $\times 10^{-7}$ are inferred from the pure absorption models, showing little trend with temperature. However, a jump in the CO_2 abundance for $T \sim 300$ K of about two orders of magnitude is seen toward AFGL 2591, but not toward NGC 7538 IRS9. This suggests that only the warmer, more evolved sources show a jump in the CO_2 abundance.
- The results from the detailed radiative transfer models including a temperature and density gradient indicate that the CO_2 abundance increases with temperature and evolutionary state. Together with the increasing gas/solid ratio and CO_2 excitation temperature, this makes gas-phase CO_2 a useful evolutionary tracer for massive protostars.
- The inferred gas-phase CO_2 abundance toward NGC 7538 IRS9 can be explained by quiescent gas-phase chemistry in the cold outer envelope with possible freeze-out.
- The high observed gas-phase CO_2 abundance for $T > 300$ K in combination with the low abundance of $\sim 10^{-8}$ for $T < 300$ K toward AFGL 2591 cannot be explained by grain-mantle evaporation or gas-phase chemistry. The low abundance for $T \sim 100$–300 K is best explained by destruction of CO_2 through the passage of a shock in the past. The high abundance in the interior is best explained by either enhanced formation of OH through X-ray ionization, producing abundant CO_2 through its reaction with CO, or incomplete destruction of evaporated CO_2 for $T > 300$ K.
- The fact that the highest inferred gas-phase CO_2 abundance is still a factor of $\sim$10 lower than the observed CO_2 ice abundances in cold sources where the ice has not yet

evaporated, suggests that CO_2 is originally formed on grain surfaces rather than by freeze-out of CO_2 gas.

Acknowledgements. This work was supported by the NWO grant 614-41-003, a Spinoza grant, and a grant from the Research Corporation (SDD). The authors would like to thank W. Schutte for providing the CO_2 ice column density toward MonR2 IRS3 and X. Tielens for useful comments.

References

Allen, D. C., Scragg, T., & Simpson, C. J. S. M. 1980, Chem. Phys., 51, 279
Anthony-Twarog, B. J. 1982, AJ, 87, 1213
Azcarate, I. N., Cersosimo, J. C., & Colomb, F. R. 1986, Rev. Mex. Astron. Astrofis., 13, 15
Boogert, A. C. A., Ehrenfreund, P., Gerakines, P. A., et al. 2000, A&A, 353, 349
Boonman, A. M. S., van Dishoeck, E. F., Lahuis, F., Wright, C. M., & Doty, S. D. 2000, in ISO beyond the Peaks, ESA SP-456, 67 [astro-ph/0105249]
Boonman, A. M. S., Stark, R., van der Tak, F. F. S., et al. 2001, ApJ, 553, L63
Boonman, A. M. S., & van Dishoeck, E. F. 2003, A&A, submitted
Boonman, A. M. S., van Dishoeck, E. F., Lahuis, F., et al. 2003, A&A, 399, 1047
Cami, J., Yamamura, I., de Jong, T., et al. 2000, A&A, 360, 562
Charnley, S. B. 1997, ApJ, 481, 396
Charnley, S. B., & Kaufman, M. J. 2000, ApJ, 529, L111
Charnley, S. B., Rodgers, S. D., & Ehrenfreund, P. 2001, A&A, 378, 1024
Dartois, E., d'Hendecourt, L., Boulanger, F., et al. 1998, A&A, 331, 651
de Graauw, T., Whittet, D. C. B., Gerakines, P. A., et al. 1996, A&A, 315, L345
D'Hendecourt, L., Jourdain de Muizon, M., Dartois, E., et al. 1996, A&A, 315, L365
Doty, S. D., van Dishoeck, E. F., van der Tak, F. F. S., & Boonman, A. M. S. 2002, A&A, 389, 446
Fraser, H. J., Collings, M. P., McCoustra, M. R. S., & Williams, D. A. 2001, MNRAS, 327, 1165
Gerakines, P. A., Whittet, D. C. B., Ehrenfreund, P., et al. 1999, ApJ, 522, 357
Giannakopoulou, J., Mitchell, G. F., Hasegawa, T. I., Matthews, H. E., & Maillard, J.-P. 1997, ApJ, 487, 346
Helmich, F.P., Jansen, D. J., de Graauw, Th., Groesbeck, T. D., & van Dishoeck, E. F. 1994, A&A, 283, 626
Helmich, F. P., & van Dishoeck, E. F. 1997, A&AS, 124, 205
Henning, Th., Pfau, W., & Altenhoff, W. J. 1990, A&A, 227, 542
Henning, T., Chini, R., & Pfau, W. 1992, A&A, 263, 285
Hogerheijde, M. R., & van der Tak, F. F. S. 2000, A&A, 362, 697
Justtanont, K., Feuchtgruber, H., de Jong, T., et al. 1998, A&A, 330, L17
Keane, J. V., Boonman, A. M. S., Tielens, A. G. G. M., & van Dishoeck, E. F. 2001a, A&A, 376, L5
Keane, J. V., Tielens, A. G. G. M., Boogert, A. C. A., Schutte, W. A., & Whittet, D. C. B. 2001b, A&A, 376, 254
Kohno, M., Koyama, K., & Hamaguchi, K. 2002, ApJ, 567, 423
Lacy, J. H., Knacke, R., Geballe, T. R., & Tokunaga, A. T. 1994, ApJ, 428, L69
Lahuis, F., & van Dishoeck, E. F. 2000, A&A, 355, 699
Lellouch, E., Bézard, B., Moses, J. I., et al. 2002, Icarus, 159, L112
Maret, S., Ceccarelli, C., Caux, E., Tielens, A. G. G. M., & Castets, A. 2002, A&A, 395, 573
Mitchell, G. F., Maillard, J.-P., Allen, M., Beer, R., & Belcourt, K. 1990, ApJ, 363, 554
Nummelin, A., Whittet, D. C. B., Gibb, E. L., Gerakines, P. A., & Chiar, J. E. 2001, ApJ, 558, 185
Persi, P., Ferrari-Toniolo, M., & Spinoglio, L. 1987, in Circumstellar matter, ed. I. Appenzeller, & C. Jordan (Dordrecht: Reidel), IAU Symp., 122, 93
Preibisch, T., Balega, Y. Y., Schertl, D., & Weigelt, G. 2002, A&A, 392, 945
Sandford, S. A., Bernstein, M. P., Allamandola, L. J., Goorvitch, D., & Teixeira, T. C. V. S. 2001, ApJ, 548, 836
Schreyer, K., Henning, Th., van der Tak, F. F. S., Boonman, A. M. S., & van Dishoeck, E. F. 2002, A&A, 394, 561
Talbi, D., & Herbst, E. 2002, A&A, 386, 1139
Thompson, R. I., Thronson, H. A., Jr., & Campbell, B. G. 1981, ApJ, 249, 622
van der Tak, F. F. S., & van Dishoeck, E. F. 2000, A&A, 358, L79
van der Tak, F. F. S., van Dishoeck, E. F., & Caselli, P. 2000a, A&A, 361, 327
van der Tak, F. F. S., van Dishoeck, E. F., Evans, N. J., II, & Blake, G. A. 2000b, ApJ, 537, 283
van der Tak, F. F. S., Boonman, A. M. S., Braakman, R., & van Dishoeck, E. F. 2003, A&A, submitted
van Dishoeck, E. F., Helmich, F. P., de Graauw, T., et al. 1996, A&A, 315, L349
van Dishoeck, E. F. 1998, in Chemistry and Physics of Molecules and Grains in Space, Faraday Discussions, 109, 31
van Dishoeck, E. F., & van der Tak, F. F. S. 2000, in Astrochemistry: From Molecular Clouds to Planetary Systems, ed. Y. C. Minh, & E. F. van Dishoeck (San Francisco: Astron. Soc. Pac.), IAU Symp., 197, 97
Wilms, J., Allen, A., & McCray, R. 2000, ApJ, 542, 914